© 2019. Published by The Company of Biologists Ltd | Journal of Cell Science (2019) 132, jcs228296. doi:10.1242/jcs.228296

SHORT REPORT

IFT25 is required for the construction of the trypanosome flagellum

Diego Huet*, Thierry Blisnick, Sylvie Perrot and Philippe Bastin‡

ABSTRACT

Intraflagellar transport (IFT), the movement of protein complexes responsible for the assembly of cilia and flagella, is remarkably conserved from protists to humans. However, two IFT components (IFT25 and IFT27) are missing from multiple unrelated eukaryotic species. In mouse, IFT25 (also known as HSPB11) and IFT27 are not required for assembly of several cilia with the noticeable exception of the flagellum of spermatozoa. Here, we show that the *Trypanosoma brucei* IFT25 protein is a proper component of the IFT-B complex and displays typical IFT trafficking. By performing bimolecular fluorescence complementation assays, we reveal that IFT25 and IFT27 interact within the flagellum in live cells during the IFT process. IFT25-depleted cells construct tiny disorganised flagella that accumulate IFT-B proteins (with the exception of IFT27, the binding partner of IFT25) but not IFT-A proteins. This phenotype is comparable to the one following depletion of IFT27 and shows that IFT25 and IFT27 constitute a specific module that is necessary for proper IFT and flagellum construction in trypanosomes. Possible reasons why IFT25 and IFT27 would be required for only some types of cilia are discussed.

KEY WORDS: Cilia, Flagella, Intraflagellar transport, Trypanosome, IFT25, IFT27, Spermatozoa

INTRODUCTION

Cilia and flagella are conserved across eukaryotes and perform variable functions. Intraflagellar transport (IFT) is the movement of protein particles or trains that deliver precursors at the tip of the organelle for assembly (Craft et al., 2015; Kozminski et al., 1993). Trains are polymers made of two protein complexes termed IFT-A and IFT-B (Cole et al., 1998; Piperno and Mead, 1997; Taschner and Lorentzen, 2016). Inhibition of IFT blocks cilia construction in all species investigated to date. In general, absence of an IFT-A protein interferes with retrograde transport, leading to the formation of short cilia that accumulate IFT proteins whereas absence of an IFT-B protein results in failure to construct the organelle (Absalon et al., 2008b; Blacque et al., 2006; Efimenko et al., 2006; Iomini et al., 2009).

An exception to the IFT conservation is IFT25 (also known as HSPB11 in mammals), which is missing from the genome of 15 ciliated species (van Dam et al., 2013). IFT25 was identified as a candidate chaperone protein based on some sequence homology with heat-shock proteins (Bellyei et al., 2007). However, this was not supported by structural analysis of the *Chlamydomonas* IFT25 protein (Bhogaraju et al., 2011). IFT25 associates with the small G protein IFT27 and is added to the IFT-B complex prior to IFT activation (Bhogaraju et al., 2011; Taschner et al., 2014; Wang et al., 2009). The absence of IFT25 in multiple species raises the question of its actual role. In contrast to other *IFT* genes, mice with deletion of the IFT25-encoding gene are viable until birth. Cilia in the lung and in the trachea are present and exhibit a normal morphology, suggesting that the protein is not essential for cilia assembly. Embryonic fibroblasts of the *Ift25* mutant contained all examined IFT proteins with the exception of IFT27 (Keady et al., 2012). Nevertheless, embryos died at birth with multiple defects related to dysfunctions in hedgehog signalling. The distribution of components of this signalling pathway was drastically modified, leading to a model where IFT25 and IFT27 would contribute to the transport of signalling molecules via the BBSome complex (Eguether et al., 2014; Keady et al., 2012; Liew et al., 2014). Accordingly, a point mutation in the human *IFT27* gene has been shown to result in Bardet–Biedl Syndrome (Aldahmesh et al., 2014). By contrast, a predicted biallelic loss of IFT27 led to a much more severe ciliopathy in a foetus (Quelin et al., 2018). Intriguingly, IFT25 is conserved in algae and multiple protists where the hedgehog cascade is absent, raising the question of its role in these organisms. Inhibition of IFT25 expression in *Chlamydomonas* did not visibly affect either IFT or flagellum construction but perturbed BBSome trafficking (Dong et al., 2017).

In an effort to clarify the function of IFT25, we investigated its function in the protist *Trypanosoma brucei*, another model for flagellum construction (Vincensini et al., 2011). The 22 *IFT* genes are conserved in *T. brucei*, IFT trafficking was demonstrated and inhibition of *IFT* gene expression severely impedes flagellum construction (Absalon et al., 2008b; Blisnick et al., 2014; Buisson et al., 2013; Davidge et al., 2006; Franklin and Ullu, 2010; Kohl et al., 2003). Here, we show that the trypanosome IFT25 is a bona fide member of the IFT-B complex, that it undergoes IFT trafficking in interaction with IFT27, and that it is essential for retrograde transport.

RESULTS AND DISCUSSION

IFT25 associates to the IFT-B complex and traffics inside the trypanosome flagellum

In *T. brucei*, IFT25 was detected in purified intact flagella of both insect (Subota et al., 2014) and bloodstream (Oberholzer et al., 2011) stages but not in detergent and salt-extracted flagellar fractions (Broadhead et al., 2006), indicative of an association to the flagellum matrix. To investigate its exact localisation, a GFP::IFT25 fusion was expressed. Western blot analysis using an anti-GFP antibody showed a single band migrating between the 37 and the 50 kDa markers, in agreement with the expected mass of the fusion protein (45 kDa) (Fig. 1A). The anti-GFP antibody was used in double immunofluorescence assays (IFA) with the anti-IFT27 antibody revealing spots along the flagellum that were stained by both antibodies (Fig. 1B).

IFT25 and IFT27 were not found in IFT-B complex purification, possibly because of their small size (Franklin and Ullu, 2010). To

Sorbonne université, École doctorale complexité du vivant, ED 515, 7 Quai Saint-Bernard, case 32, 75252 Paris cedex 05, France.
*Present address: Whitehead Institute for Biomedical Research, 455 Main Street, Cambridge, MA 02142-1479, USA.

‡Author for correspondence (philippe.bastin@pasteur.fr)

P.B., 0000-0002-3042-8679

Received 26 November 2018; Accepted 21 January 2019

Journal of Cell Science (2019) 132, jcs228296. doi:10.1242/jcs.228296

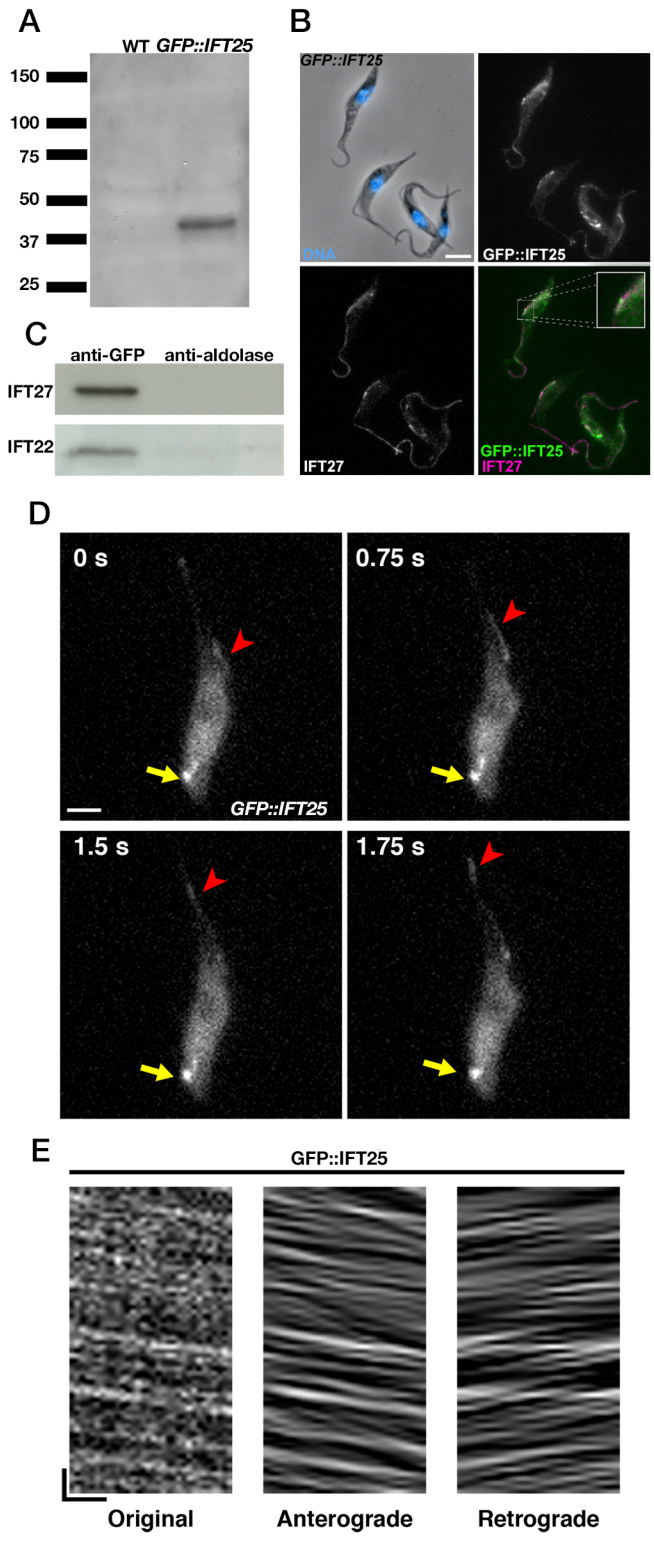

Fig. 1. IFT25 is an IFT-B protein that displays IFT. (A) Western blot of cell extracts from wild-type or GFP::IFT25 trypanosomes probed with an anti-GFP antibody. (B) IFA of cells expressing GFP::IFT25 stained with the anti-GFP antibody. Panels show the phase-contrast image merged with DAPI, and the anti-GFP, the anti-IFT27 antibody and merged images as indicated, with magnification of the flagellum showing partial colocalisation of anti-GFP and anti-IFT27 signals. Scale bar: 5 µm. (C) Immunoprecipitates of total protein extracts from cells expressing GFP::IFT25 by an anti-GFP antibody or anti-aldolase antibody. Immunoblots were performed with anti-IFT27 or the anti-IFT22 antibody. These results were replicated in two independent experiments. (D) Still images of a trypanosome expressing GFP::IFT25. The yellow arrow shows the fluorescent protein pool at the flagellum base and red arrowheads indicate the successive position of an anterograde IFT train at the indicated times. Scale bar: 2 µm. (E) Kymograph from the same sequence shows typical IFT traces for GFP::IFT25. Horizontal scale bar is 2 µm and vertical scale bar is 2 s.

establish whether IFT25 was a member of the IFT-B complex, immunoprecipitation experiments were carried out on whole-cell extracts from trypanosomes expressing GFP::IFT25. Protein lysates were immunoprecipitated with either an anti-GFP antibody or an anti-aldolase as a control. Precipitates were analysed by western blotting with antibodies against either IFT22 (Adhiambo et al., 2009) or IFT27 (Huet et al., 2014), two recognised members of the IFT-B complex. The anti-GFP antibody successfully immunoprecipitated IFT22 and IFT27, in contrast to the anti-aldolase antibody (Fig. 1C). These results reveal that IFT25 is a member of the IFT-B complex in trypanosomes.

To further link IFT25 to intraflagellar transport, live cells expressing GFP::IFT25 were observed by video microscopy. Transport in the anterograde direction was easily detected, whereas retrograde transport was more discrete but clearly present upon separation (Movie 1; still images are shown in Fig. 1D). Kymograph analyses (Fig. 1E) determined a mean (±s.d.) anterograde velocity of 2.7±0.66 µm/s (n=229), while mean retrograde velocity was 3.1 ±0.90 µm/s (n=296). Similar values have been observed for fusion proteins with IFT52 (Buisson et al., 2013), IFT81 (Bertiaux et al., 2018; Bhogaraju et al., 2013) or IFT27 (Huet et al., 2014).

Since immunoprecipitations were performed on whole-cell extracts, we used bimolecular fluorescence complementation assays (Kerppola, 2008) to investigate where IFT25 and IFT27 interact. This approach had been used successfully for interactions between IFT proteins or IFT proteins and transition fibre components in *C. elegans* (Wei et al., 2013; Yi et al., 2017). We fused the N-terminal portion of YFP spanning the first 155 amino acids (aa) to IFT25 and its C-terminal portion (aa 156–239) to IFT27. Constructs were designed for endogenous tagging at the N-terminal end of each protein, ensuring appropriate control of expression (Kelly et al., 2007). Expression of each protein individually did not lead to visible fluorescence in live cells but could be detected by IFA using a rabbit polyclonal antibody against GFP (Fig. 2A,B). By contrast, fluorescent signals and typical IFT movements were easily detected in live cells when both proteins were co-expressed (Movie 2; still images are shown in Fig. 2C). We conclude that IFT25 is a genuine component of the IFT-B complex in *T. brucei* because: (1) it is found within the matrix of the flagellum and concentrates at its base, (2) it traffics in both anterograde and retrograde directions at a speed and frequency similar to those reported for other IFT proteins, and (3) it is associated with other IFT-B proteins as shown by immunoprecipitation and bimolecular fluorescence complementation assays.

IFT25 is needed for flagellar assembly in *T. brucei*

To evaluate the role of IFT25 in *T. brucei*, an inducible RNA interference (RNAi) approach was used. The first phenotype of the $IFT25^{RNAi}$ cell line was an obvious growth defect upon depletion of the protein (Fig. S1). Scanning electron microscopy analysis of non-induced cells showed the conventional morphology with elongated cells and a long flagellum (Fig. 3A) whereas growth of $IFT25^{RNAi}$ cells in RNAi conditions for 24 (Fig. 3B) or 48 h (Fig. 3C) resulted in small cells with short flagella. $IFT25^{RNAi}$ cells were fixed and prepared for transmission electron microscopy (TEM) analysis. Sections through flagella or their base exhibited their normal aspect in control non-induced $IFT25^{RNAi}$ cells with a normal basal body,

Journal of Cell Science (2019) 132, jcs228296. doi:10.1242/jcs.228296

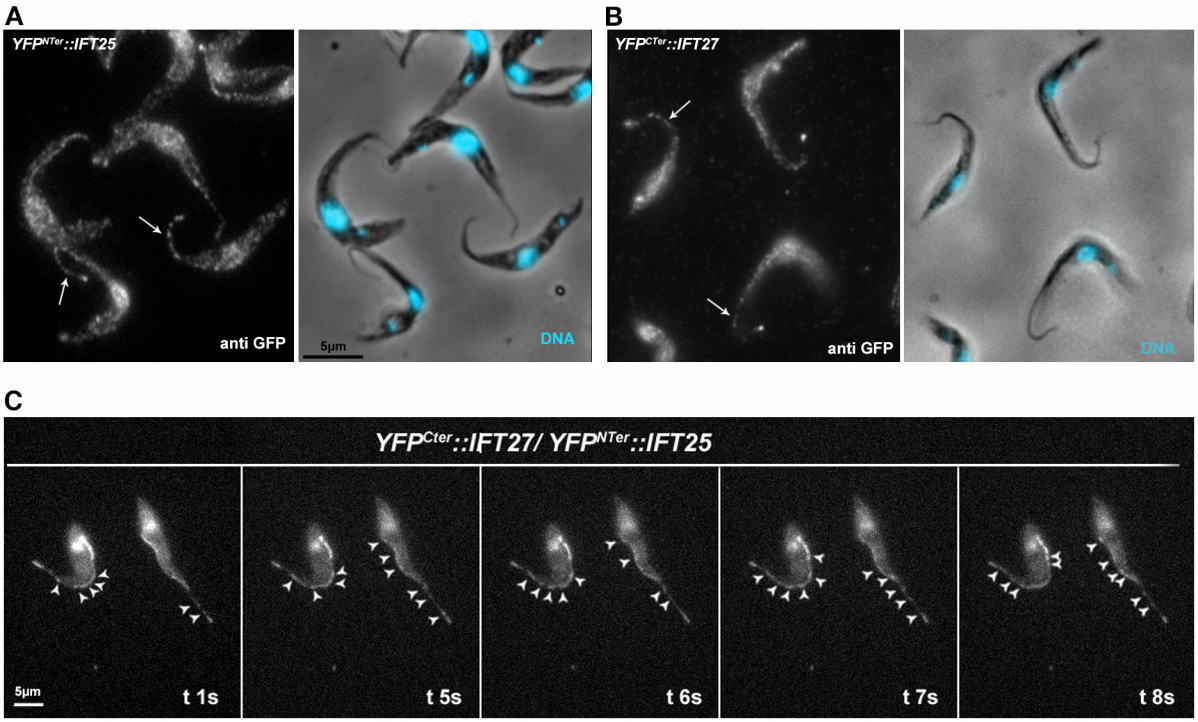

Fig. 2. Bimolecular fluorescence complementation assay shows that IFT25 and IFT27 interact and traffic together during IFT. (A,B) Expression of the YFP N-terminal portion fused to IFT25 (A) or the YFP C-terminal portion fused to IFT27 (B) individually was detected by means of a polyclonal anti-GFP antiserum. The left panels show the immunofluorescence with the anti-GFP antibody and the right panels show the phase-contrast image together with the DAPI signal. The arrows indicate flagella with a clear IFT signal pattern. (C) Bimolecular fluorescence complementation shows the interaction between IFT25 and IFT27 in the flagellum as IFT trains (arrowheads). See Movie 2 for corresponding sequence.

the transition zone and axoneme (Fig. 3D). By contrast, the flagella of induced cells were very short, and their microtubule doublets looked disorganised with a large amount of amorphous material accumulated towards the distal end (Fig. 3E–G). Small vesicles were frequently detected among this material. This is reminiscent of a defect in retrograde transport in *T. brucei* (Absalon et al., 2008a; Blisnick et al., 2014). A similar phenotype was reported for IFT22 (Adhiambo et al., 2009) and IFT27 (Huet et al., 2014), the two small G protein members of the IFT-B complex.

IFT25 and IFT27 depend on each other for access to the flagellum

We analysed the fate of IFT proteins in the *IFT25*^{RNAi} cell line. Upon induction, no changes of the total steady-state amounts of IFT-B members IFT22, IFT27 or IFT172 were observed by western blotting (Fig. 4A). IFA using the anti-IFT27 antibody showed that the protein is found in the cytoplasm upon depletion of IFT25 and therefore fails to access the flagellum (Fig. 4B). To evaluate the inverse relationship, GFP::IFT25 was expressed in the *IFT27*^{RNAi} cell line and its distribution was investigated by IFA with the anti-GFP antibody. GFP::IFT25 was found in the flagellum in control conditions but was dispersed in the cytoplasm upon silencing of IFT27 (Fig. 4C). IFT27 is a small G protein and needs to bind GTP to be associated to the IFT-B complex and to access the flagellum (Huet et al., 2014). GFP::IFT25 was introduced in the *IFT27*^{RNAi} cell line expressing an RNAi-resistant version of IFT27 with point mutations locking this small G protein in the GDP-bound or GTP-bound form. In the case of the GTP-locked form, GFP::IFT25 can still associate to IFT trains (Fig. S2A), in agreement with the fact that this version can almost completely rescue the RNAi phenotype. By contrast, the GDP-locked version cannot complement the phenotype, does not associate to the IFT-B complex and is found in the cytoplasm and not in the flagellum. In these conditions, GFP::IFT25 is only present in the cytoplasm (Fig. S2B). These results show that the simultaneous presence of IFT25 and GTP-bound IFT27 is needed for their association to the IFT-B complex. This is consistent with *in vitro* and *in vivo* data in *Chlamydomonas* that showed tight interactions between IFT25 and IFT27 prior to their association to the IFT-B complex (Bhogaraju et al., 2011; Wang et al., 2009).

IFT25 absence has opposing consequences on IFT-A and IFT-B protein localisation

The flagellum composition of *IFT25*^{RNAi} cells was analysed by IFA using, simultaneously, Mab25, an antibody detecting an axoneme-specific protein (Dacheux et al., 2012), and an antibody recognising the IFT-B protein IFT172 (Absalon et al., 2008b). Both antibodies displayed the expected pattern in non-induced cells with the typical axoneme (magenta) and IFT (green) patterns (Fig. S3A). By contrast, staining of *IFT25*^{RNAi} cells where RNAi had been induced for 2 days revealed an accumulation of large amounts of IFT172 within the short flagellum (Fig. 4D). The same result was obtained with an antibody against the IFT22 protein (Fig. S4), another component of the IFT-B complex (Adhiambo et al., 2009). This is consistent with a requirement of IFT25 for retrograde transport of IFT-B proteins, as observed for IFT27 (Huet et al., 2014).

The IFT-A complex is required for retrograde transport (Absalon et al., 2008b; Iomini et al., 2009). To monitor IFT-A proteins, the *IFT25*^{RNAi} cell line was transfected with a construct allowing expression of a Tandem Tomato (TdT)::IFT140 fusion from its endogenous locus (Huet et al., 2014). In non-induced conditions, TdT::IFT140 trafficked normally within the flagellum (Movie 3;

Journal of Cell Science (2019) 132, jcs228296. doi:10.1242/jcs.228296

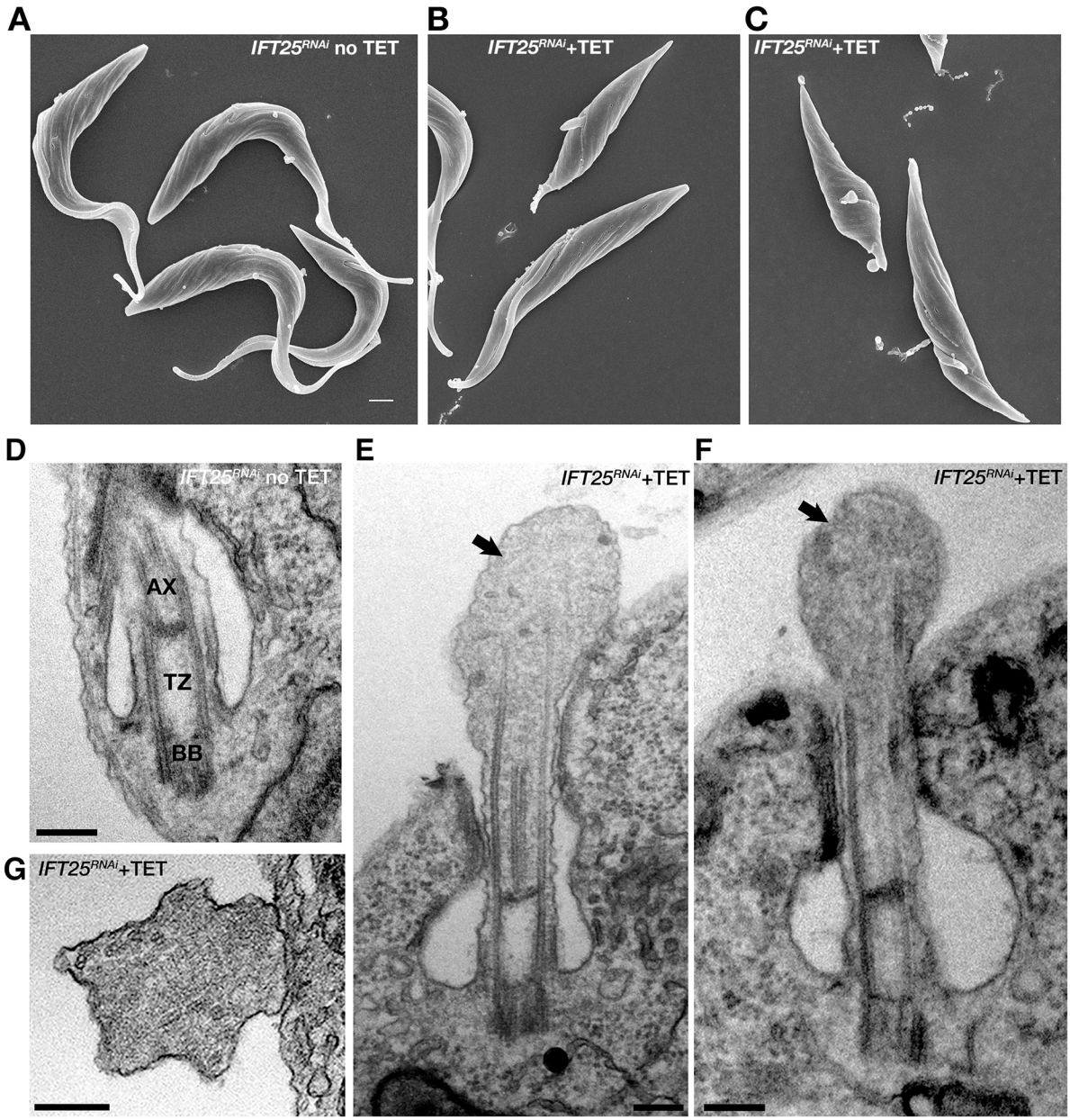

Fig. 3. Knockdown of IFT25 inhibits flagellum construction. (A–C) Scanning electron microscopy images of *IFT25*^{RNAi} cells either in non-induced conditions (A, no tet) or grown in the presence of tetracycline for 24 (B) or 48 h (C). Scale bar: 1 µm. (D–G) TEM images of sections from *IFT25*^{RNAi} cells either in non-induced conditions (D, no tet) or grown with tetracycline for 48 h (E–G). BB, basal body; TZ, the transition zone; AX, axoneme. Black arrows indicate excessive IFT-like material. Scale bars: 200 nm.

Fig. S3B). By contrast, TdT::IFT140 was immotile in induced *IFT25*^{RNAi} cells (Movie 4) and appeared to be stuck at the base of the flagellum with little or no signal within the organelle (Fig. 4E). Therefore, the absence of IFT25 prevents the recycling of the IFT-B complex while it inhibits the access of IFT-A to the flagellum. The absence of IFT-A suggests an uncoupling of IFT-B and IFT-A complexes, which could explain the observed retrograde transport phenotype. This phenotype is quite similar to what was reported upon conditional deletion of IFT25 or IFT27 in mouse male germ cells, where spermatozoa possess much shorter flagella that displayed numerous structural defects (Liu et al., 2017; Zhang et al., 2017). These include aberrant and disorganised axonemes that are too short, defects in extra-axonemal structures, such as the outer dense fibres or the fibrous sheath, and the presence of vesicles in the lumen of the flagellum. Scanning electron microscopy revealed dilation of unknown molecular composition at the distal end, leading the authors to suggest a defect in retrograde IFT (Liu et al., 2017; Zhang et al., 2017).

We propose three hypotheses to explain the different contributions of IFT25 in flagellum assembly. First, the composition of IFT trains could be different between cell types, for example as a consequence of alternative splicing or post-translational modifications. In *Chlamydomonas*, IFT25 exhibits different phosphorylation patterns and only the phosphorylated version co-sediments with IFT27 on sucrose gradients (Richey and Qin, 2012). If the trains are different, the loss of IFT25 and IFT27 could have variable consequences. Second, IFT25 and IFT27 could be required for the transport of specific cargoes that are expressed in only certain cell types such as

Journal of Cell Science (2019) 132, jcs228296. doi:10.1242/jcs.228296

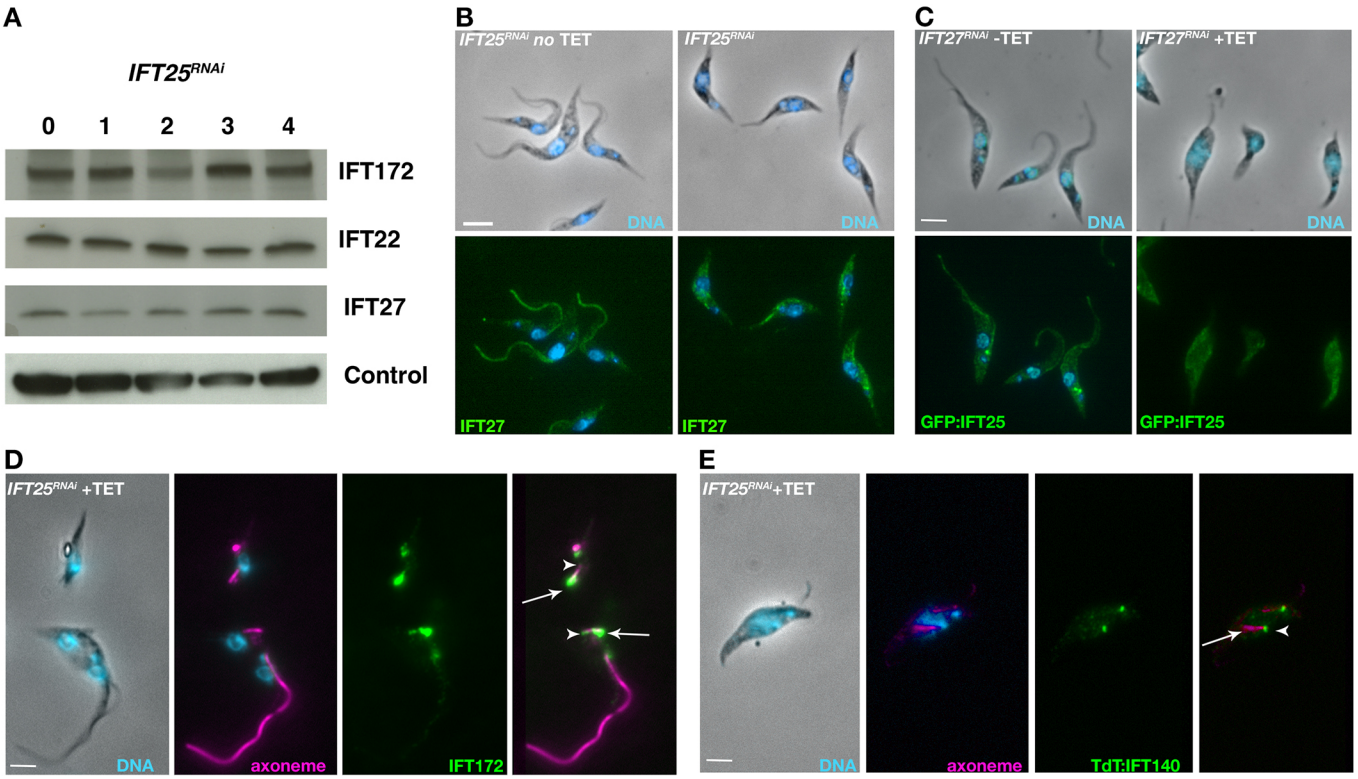

Fig. 4. Interactions between IFT25 and IFT27 and consequences on other IFT proteins. (A) Western blot with total *IFT25*^{RNAi} protein extracts in the indicated conditions. The membrane was blotted with the anti-IFT172 (top lane), anti-IFT22 (middle lane) and anti-IFT27 antibodies (bottom lane). The anti-PFR L13D6 antibody was used as a loading control. (B) *IFT25*^{RNAi} cells were non-induced (left) or induced for 3 days (right), labelled with the anti-IFT27 antibody and counterstained with DAPI. IFT27 is dispersed in the cell body. (C) *IFT27*^{RNAi} cells expressing GFP::IFT25 were non-induced (left) or induced for 3 days (right), labelled with the anti-GFP antibody and counterstained with DAPI. GFP::IFT25 is only found in the cell body in induced conditions. (D,E) Knockdown of IFT25 results in accumulation of the IFT-B protein IFT172 in the short flagellum, whereas the IFT-A protein IFT140 fails to access the flagellum. *IFT25*^{RNAi} cells (D) or *IFT25*^{RNAi} cells expressing TdTomato::IFT140 (E) were induced for 2 days, fixed in methanol, stained with the mAb25 antibody (magenta) to detect the axoneme, and the anti-IFT172 antibody (D, green) or the anti-dsRed, to detect the TdTomato::IFT140 protein (E, green), then counterstained with DAPI (cyan). Arrowheads indicate the base of the short flagellum, whereas arrows show the tip. Scale bars: 5 µm.

members of the hedgehog pathway (Keady et al., 2012; Yang et al., 2015) or the BBSome (Lechtreck et al., 2009). Of note, deletion of *BBS* genes in mouse does not have a visible impact on primary cilia in the kidney and on motile cilia in the trachea but leads to absence of the sperm flagellum (Mykytyn et al., 2004). If IFT25 and IFT27 contribute to BBS trafficking, the spermatozoa phenotype could be due to BBS perturbation. Third, trypanosome and spermatozoa flagella are characterised by the presence of extra-axonemal structures (Escalier, 2003; Portman and Gull, 2010) that could impact on the displacement of IFT trains. Alternatively, the accumulation of aberrant structures could interfere with proper IFT, and axoneme construction defects would hence be a secondary phenotype. Investigation of the role of IFT25 and IFT27 in different organisms with different types of cilia will be necessary to have a more global vision of their biological role and to understand their loss in so many species.

MATERIALS AND METHODS

Cell lines and culture conditions

All procyclic *T. brucei* cell lines were derivatives of strain 427 and grown in SDM79 medium with hemin and 10% fetal calf serum. The synthesis of the IFT25 coding sequence was conducted by GeneCust Europe (Dudelange, Luxembourg) and the synthesis product was cloned into the pPCPFR vector (Adhiambo et al., 2009) to generate the pPCPFReGFPIFT25 plasmid, allowing GFP tagging at the N-terminal end of IFT25. The resulting plasmid was linearised with NsiI, targeting integration in the intergenic region of *PFR2* (Adhiambo et al., 2009). For bimolecular fluorescence complementation assays, constructs were prepared for tagging IFT25 with the first portion of YFP and IFT27 with the second portion. If the two proteins interact closely, YFP should be reconstituted and emit light (Kerppola, 2008). The first 465 nucleotides of YFP were synthesised in a fusion at the 5′ end of the first 468 nucleotides of the IFT25 coding sequence, separated by a linker sequence (encoding GSAGSAAGSG). The resulting construct was cloned in the p2675 vector (Kelly et al., 2007) for *in situ* insertion in the *IFT25* gene upon linearisation with EcoRV and transfection in wild-type cells, resulting in the expression of the YFPNter::IFT25 protein. The final 252 nucleotides of YFP, preceded by an ATG start codon, were synthesised followed by the sequence of the Ty1 tag (Bastin et al., 1996), the linker sequence (encoding GSAGSAAGSG) and the first 440 nucleotides of the *IFT27* coding sequence, for expression of the YFP^{Cter}::IFT27 protein. The synthesised product was cloned in the p2845 vector (Kelly et al., 2007) and linearised with EcoRI to insert in the *IFT27* locus transfection in wild-type cells. Screening was carried out by IFA using a polyclonal anti-GFP antibody (cat. no. A6455, Invitrogen) to confirm the presence of each fusion protein. After this validation, the cell line expressing the YFP^{Nter}::IFT25 protein was next transfected with the construct for expression of the YFP^{Cter}::IFT27 protein and resistant cells were screened using live fluorescence imaging.

The 29-13 cell line expressing the T7 RNA polymerase and the tetracycline repressor has been described previously (Wirtz et al., 1999). For generation of the *IFT25*^{RNAi} cell line, the full *IFT25* gene (Tb927.11.13300) consisting of 471 nucleotides was chemically synthesised by GeneCust Europe and cloned in the pZJM vector (Wang et al., 2000), allowing for tetracycline-inducible expression of double-stranded (ds)RNA generating

RNAi upon transfection in the 29-13 recipient cell line. The dsRNA is expressed from two tetracycline-inducible T7 promoters facing each other in the pZJM vector. The plasmid was linearised at the unique NotI site in the rDNA intergenic targeting region before transfection (Wang et al., 2000). To monitor the interactions between IFT25 and IFT27, the pPCPFRGFPIFT25 plasmid was modified to replace the puromycin-resistance gene with a blasticidine-resistance gene to generate the pPCPFRGFPIFT25BLA vector. This plasmid was linearised with NsiI and transformed in the previously described *IFT27*^{RNAi} cell line and *IFT27*^{RNAi} cell lines expressing the RNAi-resistant versions of IFT27, IFT27T19N and IFT27Q67L (Huet et al., 2014). Trypanosomes were transfected with plasmid constructs by Nucleofector technology (Lonza, Italy) (Burkard et al., 2007). Transfectants were grown in medium with the appropriate antibiotic concentration and clonal populations were obtained by limited dilution.

Scanning and transmission electron microscopy

Cells were fixed and processed exactly as described previously (Huet et al., 2014).

Immunofluorescence and live-cell imaging

The IFA was carried out as described (Huet et al., 2014). Antibodies used were: mouse anti-IFT27 diluted 1:800 (Huet et al., 2014), mouse anti-IFT22 (1:500) (Adhiambo et al., 2009), mAb25 recognising TbSAXO1 (undiluted), a protein found all along the trypanosome axoneme (Dacheux et al., 2012), mouse monoclonal antibody anti-IFT172 (1:100) (Absalon et al., 2008b) and a commercial rabbit polyclonal anti-GFP (1:500) (Invitrogen). Subclass-specific secondary antibodies coupled to Alexa Fluor 488 and Cy3 (1:400; Jackson ImmunoResearch Laboratories, West Grove, PA) were used for double labelling. Sample observation was performed using a DMI4000 microscope (Leica) and images acquired with an ORCA-03G camera (Hamamatsu, Hamamatsu City, Japan). Pictures were analysed using ImageJ 1.47g13 software (National Institutes of Health, Bethesda, MD) and images were merged and superimposed using Adobe Photoshop CC. For live video microscopy, cells were picked up from the culture, deposited on slides and covered by a coverslip, and observed directly with the DMI4000 microscope. IFT trafficking was recorded with a 250 ms exposure per frame for 30 s using an Evolve 512 EMCCD camera (Photometrics, Tucson, AZ). Kymographs were extracted and analysed as described previously (Buisson et al., 2013; Chenouard et al., 2010).

Western blotting and immunoprecipitation

Samples were prepared and treated exactly as described previously (Huet et al., 2014). For western blots, antibodies used were the anti-IFT27 serum (1:800), the anti-IFT172 (1:500), an anti-GFP antibody (cat. no. 814-460-001, Roche, 1:500) and the monoclonal L13D6 that detects PFR proteins (Kohl et al., 1999) (1:50). For immunoprecipitation, 4 µl of polyclonal rabbit anti-GFP (cat. no. A6455, Invitrogen) or 4 µl of anti-aldolase (kind gift of Paul Michels, Edinburgh, UK) were used in a final volume of 150 µl (Huet et al., 2014).

Acknowledgements

We thank Monica Bettencourt-Dias and Esben Lorentzen for useful discussions, and Paul Michels and Derrick Robinson for the generous gift of antibodies. We thank the Ultrapole/Ultrastructural Bioimaging of the Institut Pasteur for providing access to their equipment.

Competing interests

The authors declare no competing or financial interests.

Author contributions

Conceptualization: D.H., P.B.; Methodology: D.H., T.B.; Validation: T.B.; Formal analysis: D.H.; Investigation: D.H., T.B., S.P.; Writing - original draft: D.H., P.B.; Writing - review & editing: D.H., T.B., P.B.; Visualization: D.H., P.B.; Supervision: P.B.; Project administration: P.B.; Funding acquisition: P.B.

Funding

This work is funded by Agence Nationale de la Recherche (ANR) grants (11-BSV8-016 and 14-CE35-0009-01), by a French Government Investissement d'Avenir programme, Laboratoire d'Excellence "Integrative Biology of Emerging Infectious Diseases" (ANR-10-LABX-62-IBEID) and by La Fondation pour la Recherche Médicale (Equipe FRM DEQ20150734356). Diego Huet was funded by doctoral fellowships from the French Ministry for Research and from La Fondation pour la Recherche Médicale (FDT20120925362).

Supplementary information

Supplementary information available online at
http://jcs.biologists.org/lookup/doi/10.1242/jcs.228296.supplemental

References

Absalon, S., Blisnick, T., Bonhivers, M., Kohl, L., Cayet, N., Toutirais, G., Buisson, J., Robinson, D. and Bastin, P. (2008a). Flagellum elongation is required for correct structure, orientation and function of the flagellar pocket in Trypanosoma brucei. *J. Cell Sci.* **121**, 3704-3716.

Absalon, S., Blisnick, T., Kohl, L., Toutirais, G., Doré, G., Julkowska, D., Tavenet, A. and Bastin, P. (2008b). Intraflagellar Transport and Functional Analysis of Genes Required for Flagellum Formation in Trypanosomes. *Mol. Biol. Cell* **19**, 929-944.

Adhiambo, C., Blisnick, T., Toutirais, G., Delannoy, E. and Bastin, P. (2009). A novel function for the atypical small G protein Rab-like 5 in the assembly of the trypanosome flagellum. *J. Cell Sci.* **122**, 834-841.

Aldahmesh, M. A., Li, Y., Alhashem, A., Anazi, S., Alkuraya, H., Hashem, M., Awaji, A. A., Sogaty, S., Alkharashi, A., Alzahrani, S. et al. (2014). IFT27, encoding a small GTPase component of IFT particles, is mutated in a consanguineous family with Bardet-Biedl syndrome. *Hum. Mol. Genet.* **23**, 3307-3315.

Bastin, P., Bagherzadeh, Z., Matthews, K. R. and Gull, K. (1996). A novel epitope tag system to study protein targeting and organelle biogenesis in Trypanosoma brucei. *Mol. Biochem. Parasitol.* **77**, 235-239.

Bellyei, S., Szigeti, A., Pozsgai, E., Boronkai, A., Gomori, E., Hocsak, E., Farkas, R., Sumegi, B. and Gallyas, F.Jr. (2007). Preventing apoptotic cell death by a novel small heat shock protein. *Eur. J. Cell Biol.* **86**, 161-171.

Bertiaux, E., Mallet, A., Fort, C., Blisnick, T., Bonnefoy, S., Jung, J., Lemos, M., Marco, S., Vaughan, S., Trepout, S. et al. (2018). Bidirectional intraflagellar transport is restricted to two sets of microtubule doublets in the trypanosome flagellum. *J. Cell Biol.* **217**, 4284-4297.

Bhogaraju, S., Taschner, M., Morawetz, M., Basquin, C. and Lorentzen, E. (2011). Crystal structure of the intraflagellar transport complex 25/27. *EMBO J.* **30**, 1907-1918.

Bhogaraju, S., Cajanek, L., Fort, C., Blisnick, T., Weber, K., Taschner, M., Mizuno, N., Lamla, S., Bastin, P., Nigg, E. A. et al. (2013). Molecular basis of tubulin transport within the cilium by IFT74 and IFT81. *Science* **341**, 1009-1012.

Blacque, O. E., Li, C., Inglis, P. N., Esmail, M. A., Ou, G., Mah, A. K., Baillie, D. L., Scholey, J. M. and Leroux, M. R. (2006). The WD repeat-containing protein IFTA-1 is required for retrograde intraflagellar transport. *Mol. Biol. Cell* **17**, 5053-5062.

Blisnick, T., Buisson, J., Absalon, S., Marie, A., Cayet, N. and Bastin, P. (2014). The intraflagellar transport dynein complex of trypanosomes is made of a heterodimer of dynein heavy chains and of light and intermediate chains of distinct functions. *Mol. Biol. Cell* **25**, 2620-2633.

Broadhead, R., Dawe, H. R., Farr, H., Griffiths, S., Hart, S. R., Portman, N., Shaw, M. K., Ginger, M. L., Gaskell, S. J., McKean, P. G. et al. (2006). Flagellar motility is required for the viability of the bloodstream trypanosome. *Nature* **440**, 224-227.

Buisson, J., Chenouard, N., Lagache, T., Blisnick, T., Olivo-Marin, J.-C. and Bastin, P. (2013). Intraflagellar transport proteins cycle between the flagellum and its base. *J. Cell Sci.* **126**, 327-338.

Burkard, G., Fragoso, C. M. and Roditi, I. (2007). Highly efficient stable transformation of bloodstream forms of Trypanosoma brucei. *Mol. Biochem. Parasitol.* **153**, 220-223.

Chenouard, N., Buisson, J., Bloch, I., Bastin, P. and Olivo-Marin, J. C. (2010). Curvelet analysis of kymograph for tracking bi-directional particles in flurescence microscopy images. *International Conference on Image Processing*, in press.

Cole, D. G., Diener, D. R., Himelblau, A. L., Beech, P. L., Fuster, J. C. and Rosenbaum, J. L. (1998). Chlamydomonas kinesin-II-dependent intraflagellar transport (IFT): IFT particles contain proteins required for ciliary assembly in Caenorhabditis elegans sensory neurons. *J. Cell Biol.* **141**, 993-1008.

Craft, J. M., Harris, J. A., Hyman, S., Kner, P. and Lechtreck, K. F. (2015). Tubulin transport by IFT is upregulated during ciliary growth by a cilium-autonomous mechanism. *J. Cell Biol.* **208**, 223-237.

Dacheux, D., Landrein, N., Thonnus, M., Gilbert, G., Sahin, A., Wodrich, H., Robinson, D. R. and Bonhivers, M. (2012). A MAP6-related protein is present in protozoa and is involved in flagellum motility. *PLoS One* **7**, e31344.

Davidge, J. A., Chambers, E., Dickinson, H. A., Towers, K., Ginger, M. L., McKean, P. G. and Gull, K. (2006). Trypanosome IFT mutants provide insight into the motor location for mobility of the flagella connector and flagellar membrane formation. *J. Cell Sci.* **119**, 3935-3943.

Dong, B., Wu, S., Wang, J., Liu, Y.-X., Peng, Z., Meng, D.-M., Huang, K., Wu, M. and Fan, Z.-C. (2017). Chlamydomonas IFT25 is dispensable for flagellar

assembly but required to export the BBSome from flagella. *Biol. Open* **6**, 1680-1691.

Efimenko, E., Blacque, O. E., Ou, G., Haycraft, C. J., Yoder, B. K., Scholey, J. M., Leroux, M. R. and Swoboda, P. (2006). Caenorhabditis elegans DYF-2, an orthologue of human WDR19, is a component of the intraflagellar transport machinery in sensory cilia. *Mol. Biol. Cell* **17**, 4801-4811.

Eguether, T., San Agustin, J. T., Keady, B. T., Jonassen, J. A., Liang, Y., Francis, R., Tobita, K., Johnson, C. A., Abdelhamed, Z. A., Lo, C. W. et al. (2014). IFT27 links the BBSome to IFT for maintenance of the ciliary signaling compartment. *Dev. Cell* **31**, 279-290.

Escalier, D. (2003). New insights into the assembly of the periaxonemal structures in mammalian spermatozoa. *Biol. Reprod.* **69**, 373-378.

Franklin, J. B. and Ullu, E. (2010). Biochemical analysis of PIFTC3, the Trypanosoma brucei orthologue of nematode DYF-13, reveals interactions with established and putative intraflagellar transport components. *Mol. Microbiol.* **78**, 173-186.

Huet, D., Blisnick, T., Perrot, S. and Bastin, P. (2014). The GTPase IFT27 is involved in both anterograde andretrograde intraflagellar transport. *eLife* **3**, e02419.

Iomini, C., Li, L., Esparza, J. M. and Dutcher, S. K. (2009). Retrograde intraflagellar transport mutants identify complex A proteins with multiple genetic interactions in Chlamydomonas reinhardtii. *Genetics* **183**, 885-896.

Keady, B. T., Samtani, R., Tobita, K., Tsuchya, M., San Agustin, J. T., Follit, J. A., Jonassen, J. A., Subramanian, R., Lo, C. W. and Pazour, G. J. (2012). IFT25 links the signal-dependent movement of Hedgehog components to intraflagellar transport. *Dev. Cell* **22**, 940-951.

Kelly, S., Reed, J., Kramer, S., Ellis, L., Webb, H., Sunter, J., Salje, J., Marinsek, N., Gull, K., Wickstead, B. et al. (2007). Functional genomics in Trypanosoma brucei: a collection of vectors for the expression of tagged proteins from endogenous and ectopic gene loci. *Mol. Biochem. Parasitol.* **154**, 103-109.

Kerppola, T. K. (2008). Bimolecular fluorescence complementation (BiFC) analysis as a probe of protein interactions in living cells. *Annu. Rev. Biophys.* **37**, 465-487.

Kohl, L., Robinson, D. and Bastin, P. (2003). Novel roles for the flagellum in cell morphogenesis and cytokinesis of trypanosomes. *EMBO J.* **22**, 5336-5346.

Kohl, L., Sherwin, T. and Gull, K. (1999). Assembly of the paraflagellar rod and the flagellum attachment zone complex during the Trypanosoma brucei cell cycle. *J. Eukaryot. Microbiol.* **46**, 105-109.

Kozminski, K. G., Johnson, K. A., Forscher, P. and Rosenbaum, J. L. (1993). A motility in the eukaryotic flagellum unrelated to flagellar beating. *Proc. Natl. Acad. Sci. USA* **90**, 5519-5523.

Lechtreck, K.-F., Johnson, E. C., Sakai, T., Cochran, D., Ballif, B. A., Rush, J., Pazour, G. J., Ikebe, M. and Witman, G. B. (2009). The Chlamydomonas reinhardtii BBSome is an IFT cargo required for export of specific signaling proteins from flagella. *J. Cell Biol.* **187**, 1117-1132.

Liew, G. M., Ye, F., Nager, A. R., Murphy, J. P., Lee, J. S., Aguiar, M., Breslow, D. K., Gygi, S. P. and Nachury, M. V. (2014). The intraflagellar transport protein IFT27 promotes BBSome exit from cilia through the GTPase ARL6/BBS3. *Dev. Cell* **31**, 265-278.

Liu, H., Li, W., Zhang, Y., Zhang, Z., Shang, X., Zhang, L., Zhang, S., Li, Y., Somoza, A. V., Delpi, B. et al. (2017). IFT25, an intraflagellar transporter protein dispensable for ciliogenesis in somatic cells, is essential for sperm flagella formation. *Biol. Reprod.* **96**, 993-1006.

Mykytyn, K., Mullins, R. F., Andrews, M., Chiang, A. P., Swiderski, R. E., Yang, B., Braun, T., Casavant, T., Stone, E. M. and Sheffield, V. C. (2004). Bardet-Biedl syndrome type 4 (BBS4)-null mice implicate Bbs4 in flagella formation but not global cilia assembly. *Proc. Natl. Acad. Sci. USA* **101**, 8664-8669.

Oberholzer, M., Langousis, G., Nguyen, H. T., Saada, E. A., Shimogawa, M. M., Jonsson, Z. O., Nguyen, S. M., Wohlschlegel, J. A. and Hill, K. L. (2011). Independent analysis of the flagellum surface and matrix proteomes provides insight into flagellum signaling in mammalian-infectious Trypanosoma brucei. *Mol. Cell. Proteomics* **10**, M111.010538.

Piperno, G. and Mead, K. (1997). Transport of a novel complex in the cytoplasmic matrix of Chlamydomonas flagella. *Proc. Natl. Acad. Sci. USA* **94**, 4457-4462.

Portman, N. and Gull, K. (2010). The paraflagellar rod of kinetoplastid parasites: from structure to components and function. *Int. J. Parasitol.* **40**, 135-148.

Quélin, C., Loget, P., Boutaud, L., Elkhartoufi, N., Milon, J., Odent, S., Fradin, M., Demurger, F., Pasquier, L., Thomas, S. et al. (2018). Loss of function IFT27 variants associated with an unclassified lethal fetal ciliopathy with renal agenesis. *Am. J. Med. Genet. A* **176**, 1610-1613.

Richey, E. A. and Qin, H. (2012). Dissecting the sequential assembly and localization of intraflagellar transport particle complex B in Chlamydomonas. *PLoS One* **7**, e43118.

Subota, I., Julkowska, D., Vincensini, L., Reeg, N., Buisson, J., Blisnick, T., Huet, D., Perrot, S., Santi-Rocca, J., Duchateau, M. et al. (2014). Proteomic analysis of intact flagella of procyclic Trypanosoma brucei cells identifies novel flagellar proteins with unique sub-localization and dynamics. *Mol. Cell. Proteomics* **13**, 1769-1786.

Taschner, M. and Lorentzen, E. (2016). The Intraflagellar Transport Machinery. *Cold Spring Harb Perspect Biol.* **8**.

Taschner, M., Kotsis, F., Braeuer, P., Kuehn, E. W. and Lorentzen, E. (2014). Crystal structures of IFT70/52 and IFT52/46 provide insight into intraflagellar transport B core complex assembly. *J. Cell Biol.* **207**, 269-282.

van Dam, T. J., Townsend, M. J., Turk, M., Schlessinger, A., Sali, A., Field, M. C. and Huynen, M. A. (2013). Evolution of modular intraflagellar transport from a coatomer-like progenitor. *Proc. Natl. Acad. Sci. USA* **110**, 6943-6948.

Vincensini, L., Blisnick, T. and Bastin, P. (2011). 1001 model organisms to study cilia and flagella. *Biol. Cell* **103**, 109-130.

Wang, Z., Morris, J. C., Drew, M. E. and Englund, P. T. (2000). Inhibition of trypanosoma brucei gene expression by RNA interference using an integratable vector with opposing T7 promoters. *J. Biol. Chem.* **275**, 40174-40179.

Wang, Z., Fan, Z.-C., Williamson, S. M. and Qin, H. (2009). Intraflagellar transport (IFT) protein IFT25 is a phosphoprotein component of IFT complex B and physically interacts with IFT27 in Chlamydomonas. *PLoS One* **4**, e5384.

Wei, Q., Xu, Q., Zhang, Y., Li, Y., Zhang, Q., Hu, Z., Harris, P. C., Torres, V. E., Ling, K. and Hu, J. (2013). Transition fibre protein FBF1 is required for the ciliary entry of assembled intraflagellar transport complexes. *Nat. Commun.* **4**, 2750.

Wirtz, E., Leal, S., Ochatt, C. and Cross, G. A. (1999). A tightly regulated inducible expression system for conditional gene knock-outs and dominant-negative genetics in Trypanosoma brucei. *Mol. Biochem. Parasitol.* **99**, 89-101.

Yang, N., Li, L., Eguether, T., Sundberg, J. P., Pazour, G. J. and Chen, J. (2015). Intraflagellar transport 27 is essential for hedgehog signaling but dispensable for ciliogenesis during hair follicle morphogenesis. *Development* **142**, 2860.

Yi, P., Li, W. J., Dong, M. Q. and Ou, G. (2017). Dynein-Driven Retrograde Intraflagellar Transport Is Triphasic in C. elegans Sensory Cilia. *Curr. Biol.* **27**, 1448-1461.e7.

Zhang, Y., Liu, H., Li, W., Zhang, Z., Shang, X., Zhang, D., Li, Y., Zhang, S., Liu, J., Hess, R. A. et al. (2017). Intraflagellar transporter protein (IFT27), an IFT25 binding partner, is essential for male fertility and spermiogenesis in mice. *Dev. Biol.* **432**, 125-139.

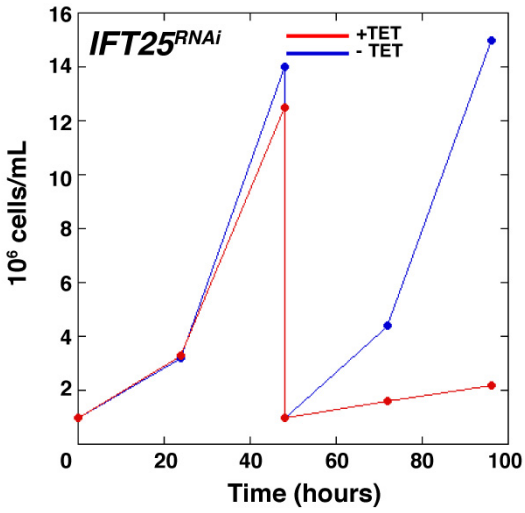

Fig. S1. IFT25 is essential for growth in *T. brucei.* Growth curve of non-induced (blue) and induced (red) *IFT25*^{RNAi} cells revealed very slow growth after two days in RNAi conditions, i.e. after the emergence of non-flagellated cells. Cells were diluted at day 2 of the experiment.

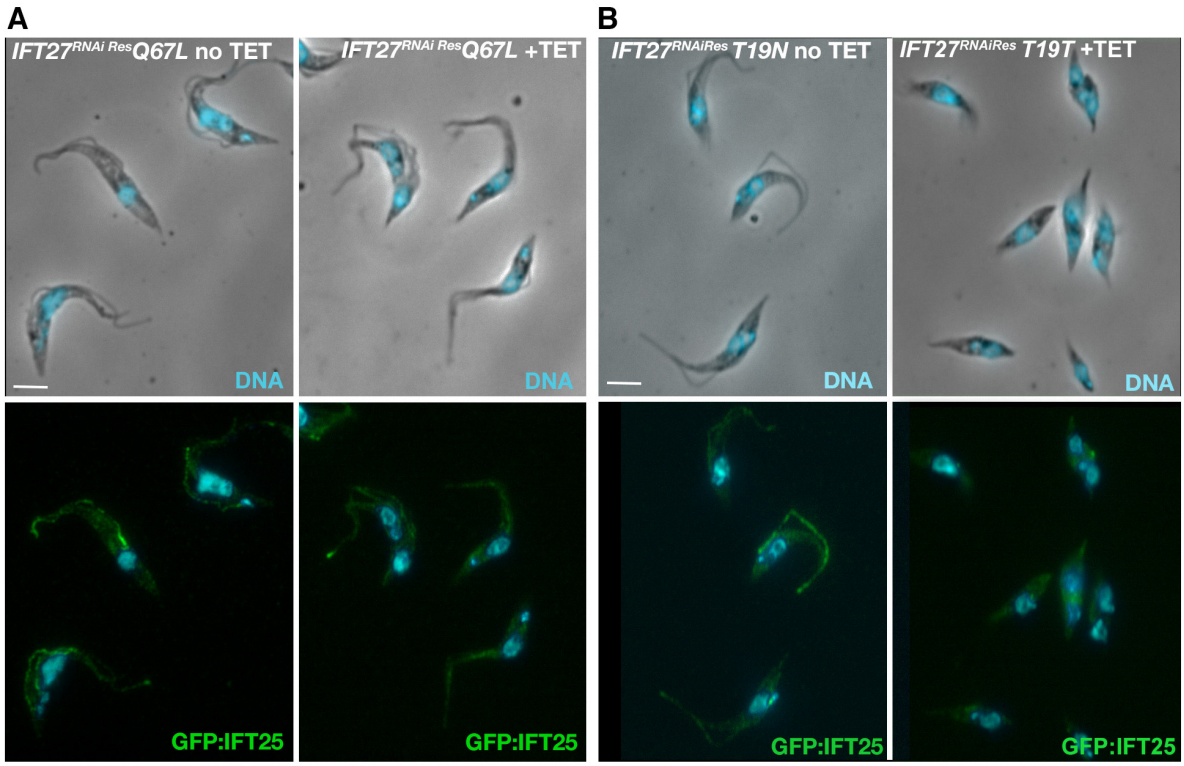

Fig. S2. IFT25 requires an IFT27 version able to associate to GTP to access the flagellum. (A) *IFT27*^{RNAi} cells expressing the RNAi resistant version of IFT27Q67L (GTP-locked state) (Huet et al., 2014) were transformed to constitutively express the GFP::IFT25 protein. Non-induced cells (left, -TET) or trypanosomes induced for 3 days (right, +TET) were labelled with the anti-GFP antibody (green) and counterstained with DAPI (cyan). GFP::IFT25 was found in the flagellum in both control and induced conditions. (B) *IFT27*^{RNAi} cells expressing the RNAi resistant version of IFT27T19N (GDP-locked state) (Huet et al., 2014) were transformed to constitutively express the GFP::IFT25 protein. Non-induced cells (left, -TET) or trypanosomes induced for 3 days (right, +TET) were labelled with the anti-GFP antibody (green) and counterstained with DAPI (cyan). GFP::IFT25 was found in the flagellum in control conditions but was only present in the cell body after depletion of the endogenous IFT27. Scale bar: 5µm.

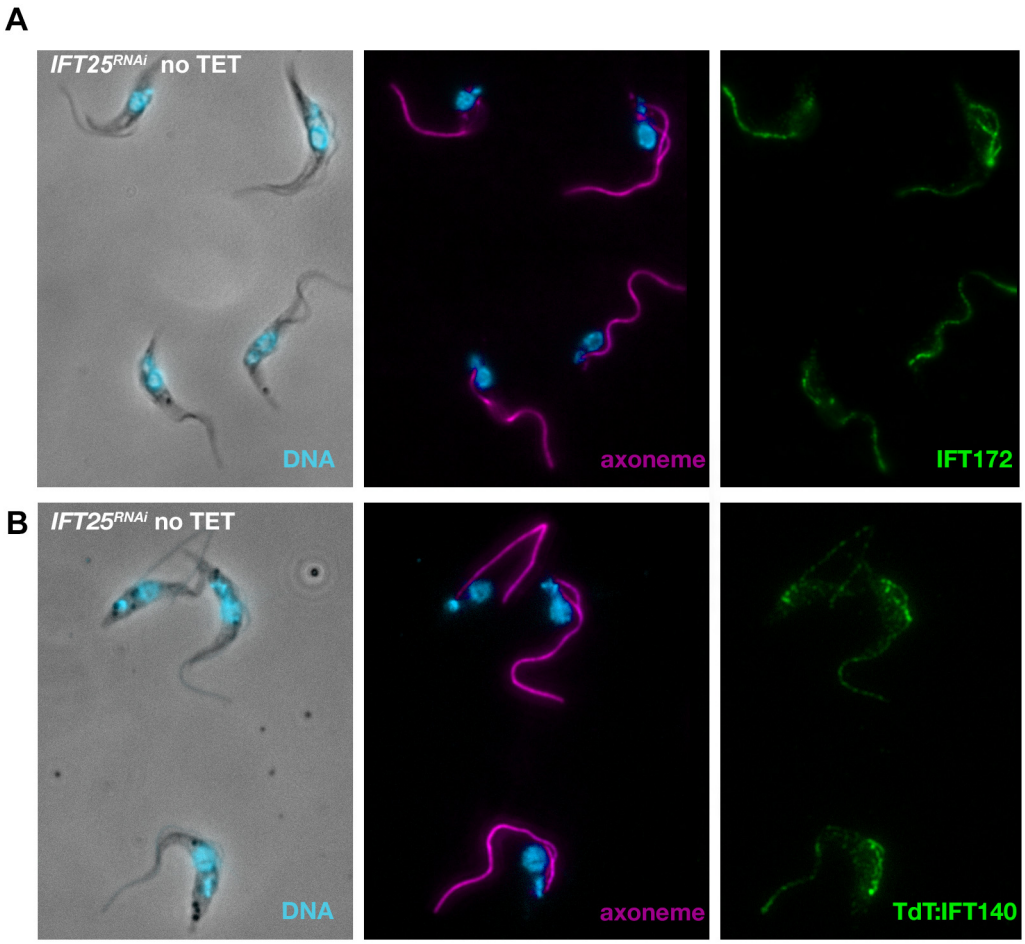

Fig. S3. Non-induced *IFT25*^{RNAi} cells display normal IFT172 and TdTomato::IFT140 distribution. (A) Non-induced *IFT25*^{RNAi} cells were fixed in methanol, stained with the mAb25 antibody (magenta) to detect the axoneme and the anti-IFT172 antibody (green), and then counterstained with DAPI (cyan). (B) Non-induced *IFT25*^{RNAi} cells expressing TdTomato::IFT140 from its endogenous locus were fixed in methanol, stained with the mAb25 antibody (magenta) to detect the axoneme and the anti-dsRed to detect the TdTomato::IFT140 protein (green), and then counterstained with DAPI (cyan).

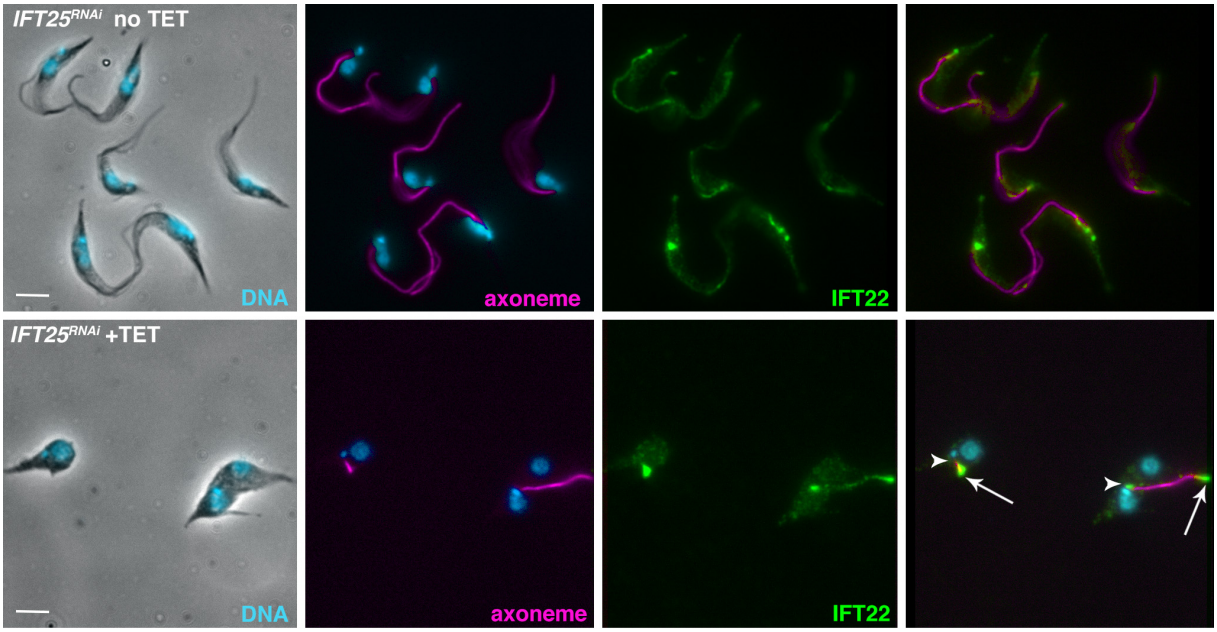

Fig. S4. Knockdown of IFT25 results in accumulation of the IFT-B protein IFT22 in the short flagellum. *IFT25*^{RNAi} cells were non-induced (top panels) or RNAi was induced for 60 hours (bottom panels), fixed in methanol, stained with the mAb25 antibody (magenta) to detect the axoneme and the anti-IFT22 antibody (green), and then counterstained with DAPI (cyan). Arrowheads indicate the base of the short flagellum whereas arrows show the tip.

Movie 1. Trypanosome expressing GFP::IFT25. IFT trafficking was recorded with a 250ms exposure per frame.

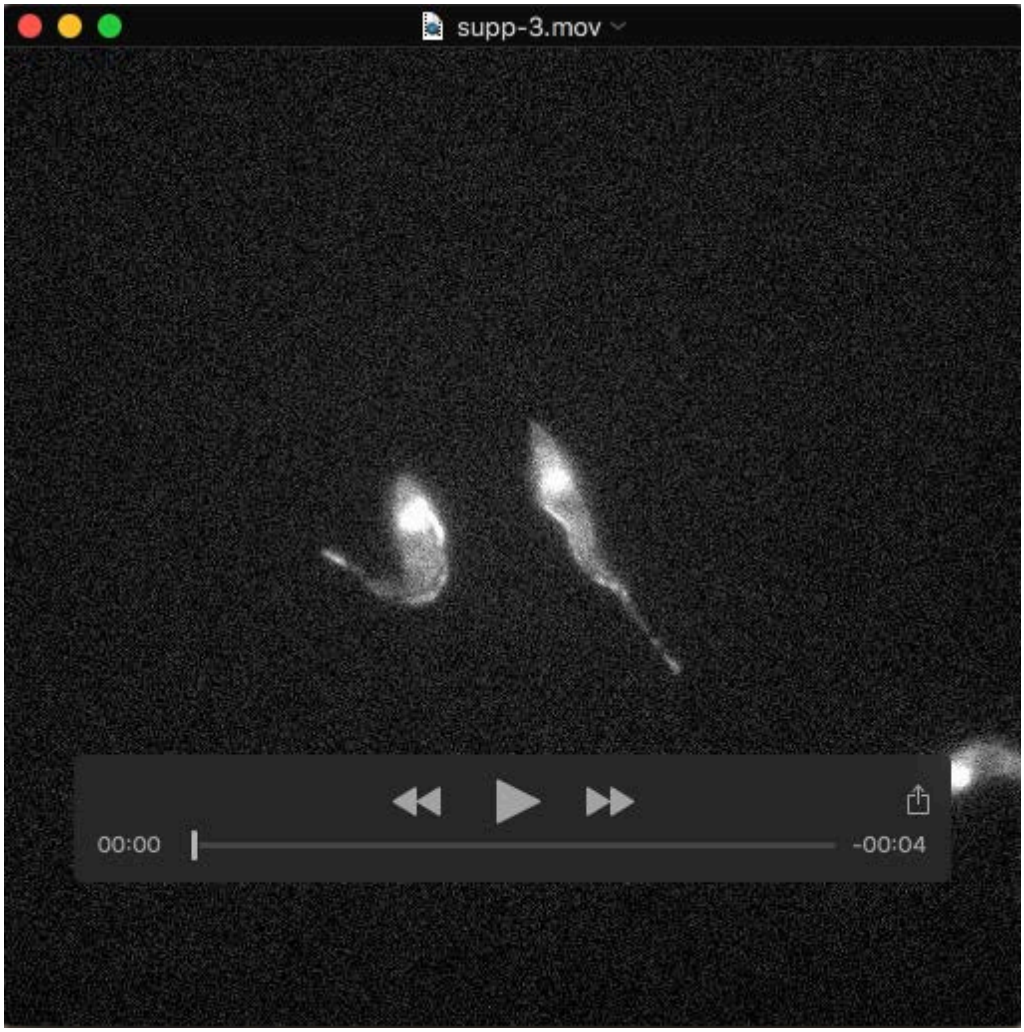

Movie 2. Trypanosomes expressing YFPNter::IFT25 and YFPCter::IFT27. IFT trafficking was recorded with a 250ms exposure per frame.

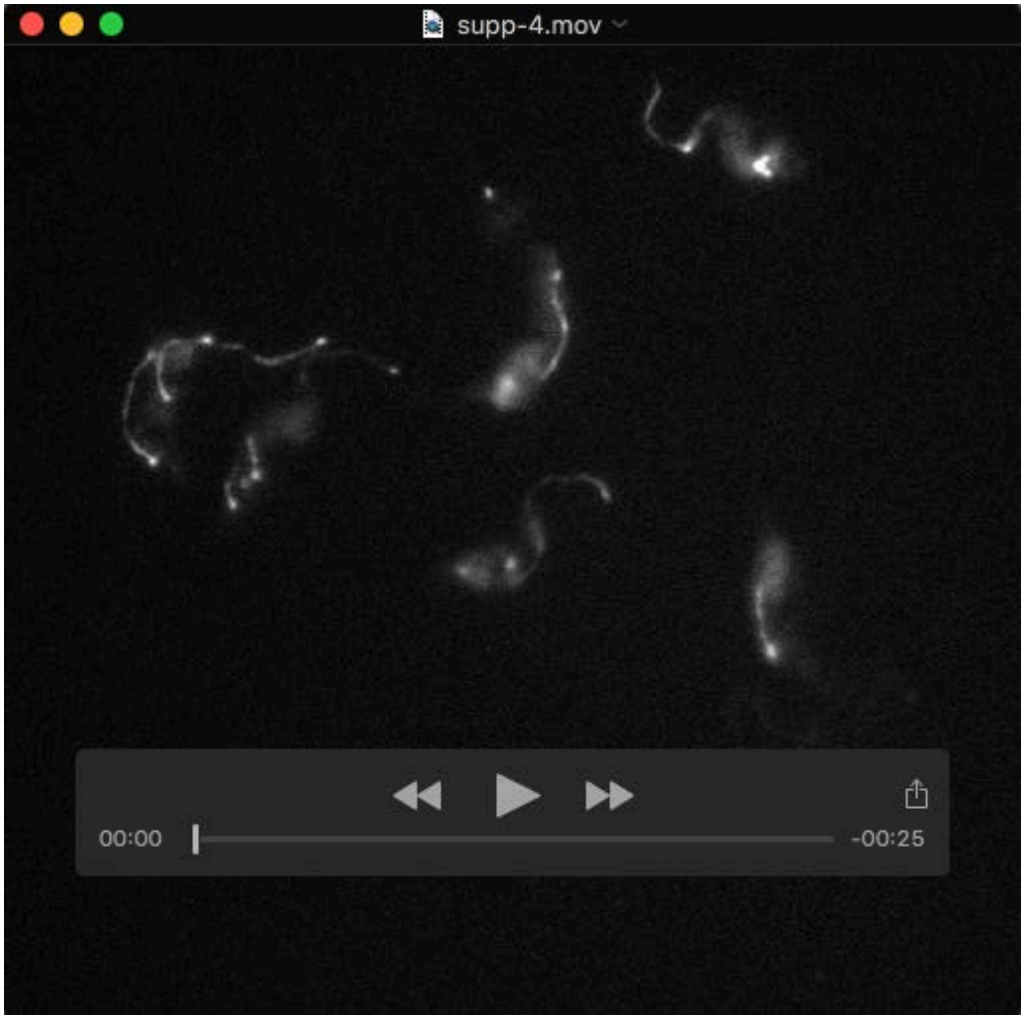

Movie 3. *IFT25*^{RNAi} cell expressing TdT::IFT140 grown in the absence of tetracycline and hence without RNAi. Robust IFT trafficking is visible in all cells.

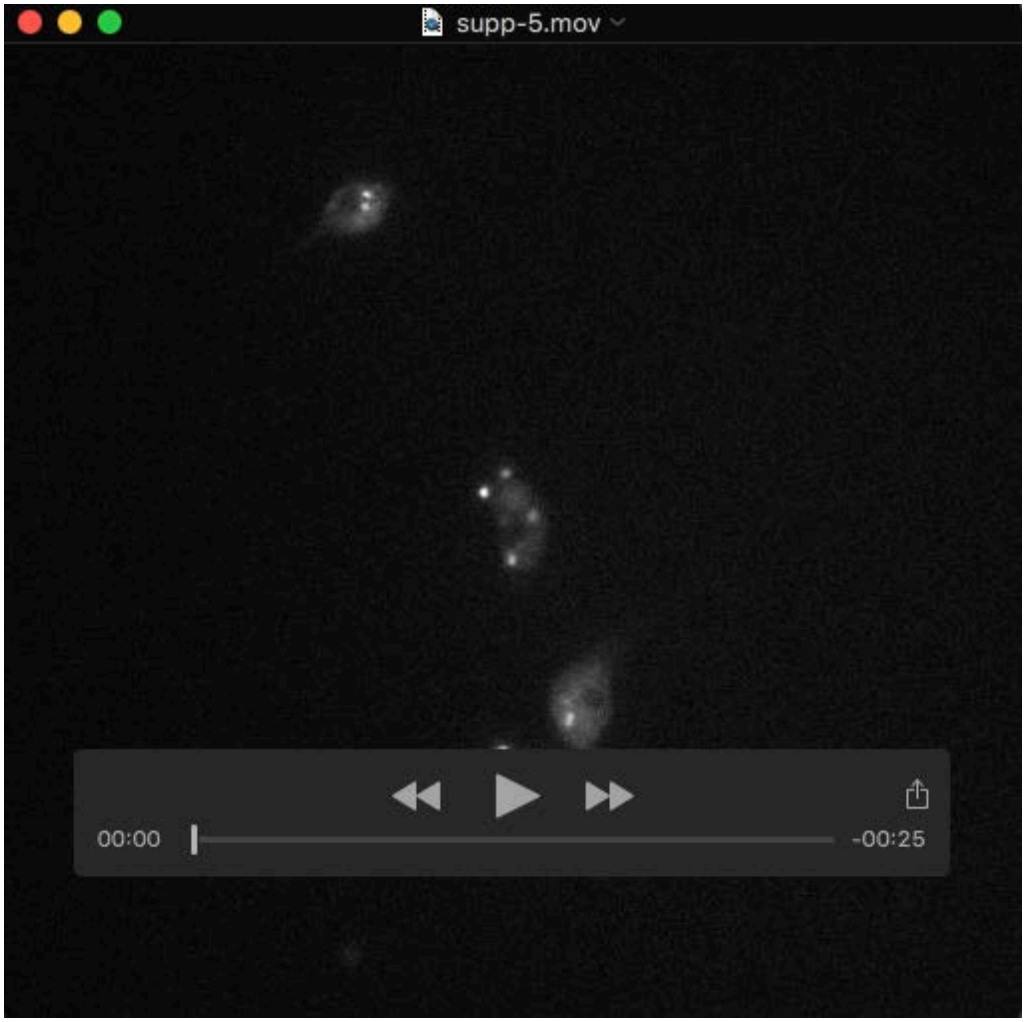

Movie 4. *IFT25*^{RNAi} cell expressing TdT::IFT140 grown in the presence of tetracycline and hence in RNAi conditions. No trafficking is observed and TdT::IFT140 appears to remain at the base of the flagella.